Hindawi
Advances in Civil Engineering
Volume 2018, Article ID 7354025, 14 pages
https://doi.org/10.1155/2018/7354025

Research Article

Crack Risk Evaluation of Submerged Concrete Tunnel during Hardening Phase

G. M. Ji,[1] **T. Kanstad**,[2] **and Ø. Bjøntegaard**[3]

[1]*SINTEF Ocean, 7450 Trondheim, Norway*
[2]*The Norwegian University of Science and Technology (NTNU), 7491 Trondheim, Norway*
[3]*Norwegian Public Roads Administration, Tunnel and Concrete Section, Oslo, Norway*

Correspondence should be addressed to G. M. Ji; guomin.ji@sintef.no

Received 5 September 2018; Accepted 13 November 2018; Published 23 December 2018

Academic Editor: Constantin Chalioris

Cracking of concrete structures during the hardening phase often seriously compromises not only structure integrity but also durability and long-term service life. Especially for large massive structures, for example, concrete submerged tunnel, the reliable crack risk evaluation at the hardening phase is critical to the successful design. Mineral additives such as silica fume (SF), blast furnace slag (BFS), and fly ash (FA) have been used extensively in production of high-performance concrete in the last decades. The mineral additives such as FA and BFS not only reduce the hydration heat during the hardening phase but also have significant influence on the development of mechanic and viscoelastic properties at an early age. The main objective of the research is to propose a design methodology to select the appropriate composition of concrete for construction of the submerged tunnel. The influence of mineral additives such as FA and BFS on the risk of cracking during the hardening phase was investigated for the massive concrete structure. Five types of concrete mixes denoted as SV40, 40% BFS, 60% BFS, 40% FA, and 60% FA concrete are considered in the current study, and the measurement to reduce the initial temperature is also considered for 60% FA concrete. First, the well-documented material models are verified by calibration of restraint stress development in the TSTM test by using the finite element method (FEM), and then the 3D thermal-structural analysis is performed to assess the cracking risk for the submerged tunnel during the hardening phase. Based on analysis results, the 60% FA concrete has both the lowest maximum temperature and the lowest stress/strength ratio, and the cracking-free design based on the current study ensures the successful construction of the submerged tunnel.

1. Introduction

In the past, prediction of the early-age cracking was almost exclusively based on temperature criteria. The temperature development in the young concrete was calculated, and cracking was predicted from the maximal temperature difference in the massive concrete structure. To avoid cracking, limitations were applied to maximum temperature and temperature difference between the surface and the center of the structure and between the new and the older adjoining structures. These limitations were based on practical experience and experience from the laboratory. The main drawback of the temperature-based crack risk estimation is that the other important factors in stress calculation are not considered: restraint conditions, material properties, and shrinkage. Several researchers [1, 2] have shown that there is no general correlation between stresses and temperature. Whether young concrete will crack or not depends very much on restraint conditions and material properties.

In North America, the second Midtown Tunnel built under the Elizabeth River from 2013 to 2016 is the first deepwater concrete immersed-tube tunnel and only the second all-concrete immersed tunnel in the U.S. The all-concrete tunnel design allows for a strong, durable structure with substantial economic savings compared to a more conventional design using a steel tube encased in concrete, and it is extensively used across Europe. The all-concrete tunnel design is also selected for the submerged tunnel built in Oslo.

Cracking during the hardening phase is prone to occur in massive concrete structures, and it compromises not only structure integrity but also durability and long-term service life. The early-age cracking was observed in concrete bridge

deck expansion joint repair sections [3]. The cracking risk at the hardening phase is the main concern in the design of the concrete submerged tunnel built in Oslo. The illustration of the submerged tunnel is shown in Figure 1. The total length of the tunnel is about 1110 m with three traffic lanes in each direction, and 675 m of it (30 sections) is submerged under the seawater.

In recent years, an increased interest in cracking of hardening concrete has led to extensive research on this subject [4–9]. A large number of material models for young concrete have been presented and implemented in computer programs for the simulation of stress development. Simulation of the hardening structure in general has to take into account temperature development due to hydration, development of material properties, and restraint conditions of the particular structure [10, 11]. FEM simulation was performed to predict early thermal stress in second lining concrete of NATM tunnels, and the model was verified by field measurements [12]. The effect of reinforcement on the early-age cracking is investigated [13], and the results showed that the probability of cracking in highly reinforced structures is lower than that has been estimated in calculations where the effect of reinforcement is completely ignored. For quantifying the effect of reinforcement on the stress development due to restrained load-independent deformations, a "strain enhancement factor" has been introduced. From the experiments with HSC specimens reinforced with four rebars, this factor reached a mean value of 1.85. A simplified model is used to investigate the possible effect of a gradient concrete material distribution in mass concrete structures on crack reduction. The results of the analysis show that gradient concrete might contribute to lowering the constraint stresses and therefore the crack risk during concrete hardening [14]. The influence of gravel (consisting mainly of quartz), basalt, granite, and limestone aggregate on the temperature development, stress level, and cracking risk has been studied in the experimental and numerical tests [15]. The use of aggregates with appropriate thermal properties in concrete such as low specific heat, high thermal conductivity coefficient, and low coefficient of thermal expansion reduces the induced stresses and the cracking risk. The reinforcement concrete structure was studied by several authors by using software DIANA, ABAQUS, ANSYS, etc. [16–18].

In the current study, a design methodology is proposed based on both comprehensive tests and advanced numerical simulations. The procedure of the design methodology is as follows:

(i) Suggest candidate concrete with different compositions
(ii) Establish material models through a comprehensive test program
(iii) Calibrate material models against temperature-stress testing machine (TSTM) tests
(iv) Perform advanced thermal-structural numerical simulation
(v) Recommend the concrete composition with lowest cracking risk

2. Candidate Concrete

The concrete proposed in the current design includes one typical construction concrete (SV40) and four other concrete types with different percentages of mineral additives (FA or BFS), and the composition of concrete is presented in Table 1. The materials tests and the mechanical properties do not include the steel reinforcement (bars, etc.).

3. Material Models

A comprehensive test program was performed at laboratories of Norwegian Public Roads Administration (SVV) and Norwegian University of Science and Technology (NTNU) to determine the following material parameters [19]:

(i) Heat of hydration
(ii) Mechanical properties (elastic modulus, compressive strength, and tensile strength)
(iii) Creep/relaxation properties under compressive loading
(iv) Volume change

3.1. Heat of Hydration. A semiadiabatic temperature test was performed to determine the hydration heat and thermal properties. The heat of hydration is expressed in the simple three-parameter equation, which is commonly used in engineering practice [20]:

$$Q = Q_{\infty} \cdot \exp\left\{-\left(\frac{\tau}{t_e}\right)^{\alpha}\right\}, \tag{1}$$

where Q_{∞} is the asymptotic value of the produced heat, while τ and α are model parameters which are determined from experimental data (Table 2). The activation energy is determined by strength development at several isothermal temperature histories. For temperature calculation, the most important input parameters, in addition to the produced heat and heat capacity, are the heat conductivity and the boundary conditions (connectivity and ambient air temperature) at the various surfaces of the structure.

3.2. Mechanical Properties. The modified version of CEB-FIP MC 1990 is used to describe the development of the compressive strength, tensile strength, and modulus of elasticity [21]:

$$f_c(t_e) = f_c(28) \cdot \left\{\exp\left[s \cdot \left(1 - \sqrt{\frac{28}{t_e - t_0}}\right)\right]\right\},$$

$$f_t(t_e) = f_t(28) \cdot \left\{\exp\left[s \cdot \left(1 - \sqrt{\frac{28}{t_e - t_0}}\right)\right]\right\}^{n_t}, \tag{2}$$

$$E_c(t_e) = E_c(28) \cdot \left\{\exp\left[s \cdot \left(1 - \sqrt{\frac{28}{t_e - t_0}}\right)\right]\right\}^{n_E},$$

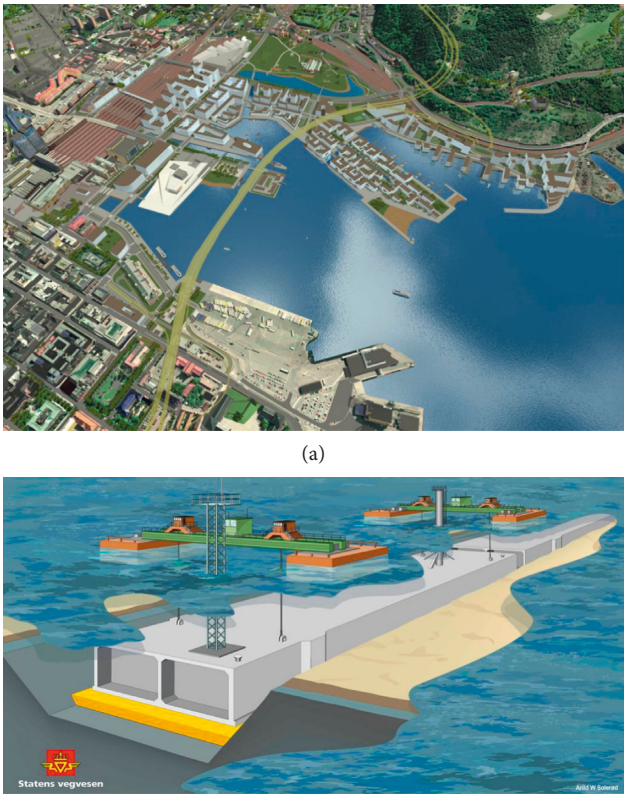

(a)

(b)

Figure 1: Bjørvika submerged tunnel.

Table 1: Concrete compositions and mechanical properties at 28 days.

Materials	Concrete fraction (kg/m^3), nominal values				
	SV40	40% BFS	60% BFS	40% FA	60% FA
Norcem Anleggsement (c)	404.1	263.4	232.5	263.7	232.9
Silica fume (s)	20.2	13.2	11.6	13.2	11.6
Fly ash (FA)	—	—	—	105.5	139.6
Blast furnace slag (BFS)	—	105.4	139.5	—	—
Water (w)	178				
Norstone 0–8 mm	910	995	994	965	958
Norstone 8–16 mm			880		
Sikament 92			1.9		
Measured values: fresh concrete					
Air (%)	4.3	1.6	1.6	1.4	1.1
Density (kg/m^3)	2370	2410	2410	2410	2370
Slump (mm)	70	125	140	150	160
Binder composition (ratio and volumes)					
s/c ratio			0.05		
FA or BFS/c ratio	—	0.40	0.60	0.40	0.60
Binder and water volume (ltr)	317	305	306	316	321
w/(c + 2s + FA + BFS) ratio	0.40	0.45	0.45	0.45	0.45

in which t_0 is introduced to identify the start of significant mechanical properties development, and it might be determined from a TSTM test; it is the time at which stiffness achieves a value high enough to produce measurable stresses. The parameter s was determined from the compressive strength development, whereas parameters n_t and n_E were determined from the tensile strength and elastic modulus tests, respectively (Table 3).

3.3. Creep in Compression. The creep of concrete at the constant moisture and thermal state may be well described by

Table 2: Parameters for thermal properties.

Concrete type	Heat production				Activation energy (1/°K)		Thermal conductivity	Specific heat
	Binder (kg/m^3)[1]	Q_∞ (kJ/kg binder)	τ (h)	α	A	B	(kJ/ms°C)	(J/kg°C)
SV40	424	319	15.04	1.34	21966	2699	0.0026	1.06
40% BFS	382	286	18.95	0.84			0.0024	
60% BFS	384	274	21.97	0.78			0.0024	
40% FA	382	244	20.12	1.39	26574	1030	0.0024	1.07
60% FA	384	215	21.86	1.17	36192	1136	0.0024	1.07
60% FA (with initial temperature 11°C)	382	222	17.34	1.15			0.0024	

[1]Binder = cement + silica fume + fly ash + blast furnace slag.

Table 3: Model parameters for mechanical properties.

Concrete	f_{c28} (MPa)	f_{t28} (MPa)	E_{c28} (MPa)	s	n_E	n_t	t_0 (hrs)
SV40	65.1	3.86	31700	0.197	0.421	0.722	8.0
40% BFS	54.8	3.89	33700	0.368	0.300	0.605	8.8
60% BFS	52.8	3.34	32200	0.433	0.327	0.604	8.8
40% FA	47.2	3.32	32900	0.363	0.253	0.623	9.5
60% FA	41.2	3.20	33360	0.418	0.251	0.561	10.5

power curves of load durations $t - t'$ and by inverse power curves of age t' at loading. This leads to the most well-known compliance function double power law [22, 23]:

$$J(t,t') = \frac{1}{E_0} + \frac{\varphi_1}{E_0}\left(t'^{-m} + \alpha\right)(t-t')^n. \quad (3)$$

The double power law (DPL) is originally proposed for hardened concrete. It was modified to describe the creep property of early-age concrete by taking into account the aging characteristics of young concrete [24, 25]:

$$J(t,t') = \frac{1}{E_c(t')}\left[1 + \varphi(t')^{-d}(t-t')^p\right], \quad (4)$$

where $J(t,t')$ = compliance function, t' = concrete age at loading (days), t = concrete age (days), $E_c(t')$ = modulus of elasticity at loading time, and φ, d, and p = creep model parameters.

From the previous study [19], it can be seen that the combined compressive and tensile creep data give best correspondence with the measured stress developments in the TSTM tests, and using only the compressive DPL parameters gives better agreement with the test results than using only the tensile DPL parameters. For the FEM program DIANA which is used in the current study, only one set of DPL parameters could be specified in the input file, and then the compressive creep data as shown in Table 4 are used in the analysis.

3.4. Volume Change. The thermal dilation (TD) and the autogenous deformation (AD), which are the driving forces to the restraint stress, were determined from the dilation rig test [26]. The sum of the two properties is measured directly and then separated into TD and AD. But this separation is only valid for that particular temperature history. The practical solution is simply to assume that the thermal dilation coefficient is a constant, and then the autogenous deformation is determined by subtracting thermal dilation from the total deformation measured under one realistic temperature history.

Table 4: Creep parameters in DPL for the compressive creep tests.

Concrete	Creep model parameters		
	φ	d	p
SV40	0.98	0.18	0.19
40% BFS	1.05	0.30	0.32
60% BFS	0.77	0.30	0.32
40% FA	1.23	0.28	0.30
60% FA	1.47	0.24	0.24

The imposed temperatures and measured total deformations for five concrete types are shown in Figure 2. The constant coefficients of thermal expansion (CTEs) used to separate AD and TD and autogenous deformation (AD) after 12 days are presented in Table 5. The separated AD and TD are also shown in Figure 2.

4. Verification of Material Models

Stress development in restraint specimens exposed to realistic temperature histories was measured in the temperature-stress testing machine (TSTM) for all five concrete types. A numerical study was performed by the 3D finite element program DIANA [27] to verify the test results.

The calculated stress developments of concrete containing 40% and 60% BFS have very good agreement with the test results, and the maximum deviation in both compression and tension is about 0.2 MPa (Figure 3). The calculated compressive stress of the concrete containing 40% and 60% FA with 20°C initial temperature is higher than the measured

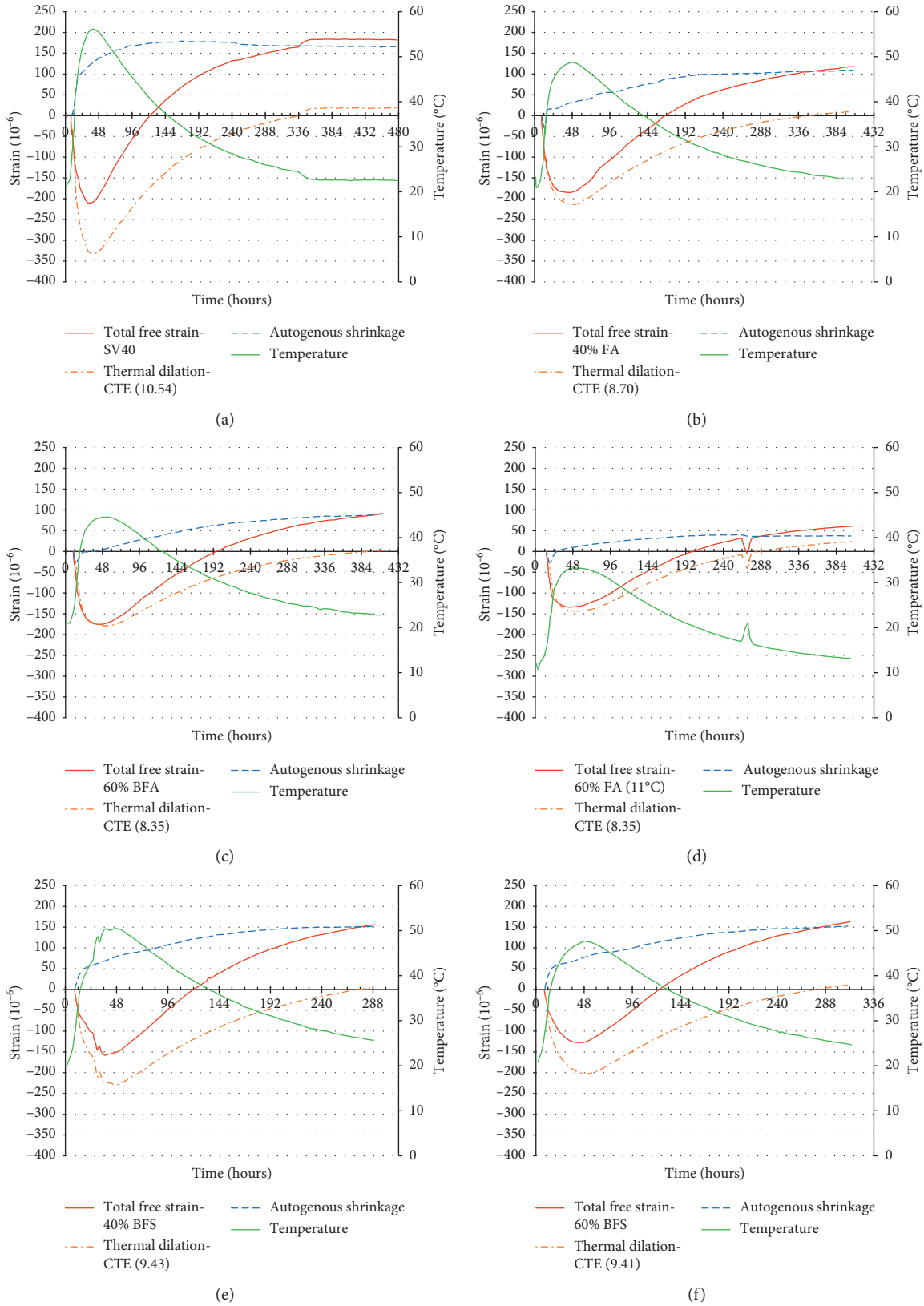

Figure 2: Free deformation and separated thermal dilation and autogenous deformation: (a) SV40; (b) 40% FA; (c) 60% FA; (d) 60% FA (11°C); (e) 40% BFS; (f) 60% BFS.

Table 5: Constant coefficient of thermal expansion (CTE) and autogenous deformation (AD) after 12 days.

Concrete type	Maximum temperature (°C)	CTE (10^{-6})	AD (10^{-6})
SV40	56.0	10.54	150
40% FA	48.7	8.70	100
60% FA	44.4	8.35	80
60% FA-11°C	33.0	8.35	38
40% BFS	50.4	9.43	152
60% BFS	47.5	9.41	150

ones, and the calculated tensile stress of the 60% FA concrete is lower than the test results, while the calculated tensile stress of the 40% FA concrete is lower than the test results at first 10 days; afterwards, it becomes higher than the test results. The calculated compressive stress and tensile stress of the 60% FA concrete with 11°C initial temperature are higher than the test results. The calculated compressive stress of the SV40 concrete is higher than the test results, and the calculated tensile stress is lower than the test results until 14 days.

All the model parameters used in the analysis were determined from independent tests, and no parameters are adjusted to achieve better fit with the test results. It can be concluded that the model parameters used in the analysis make reasonably accurate prediction of the stress development for the concrete containing different percentages of FA and BFS, but the deviation for the SV40 concrete is high especially for the tensile stress at 3 days; this is probably due to the low elastic modulus of the SV40 concrete from the test. The maximum compressive and tensile stresses are summarized in Table 6 with the maximum deviation of compressive and tensile stresses. The deviation between the calculated and measured maximum stresses after 12–17 days is less than 12%, and in most cases, the calculations overestimate the maximum tensile stresses.

5. Numerical Simulation

In the design process, the temperature and stress development in the submerged tunnel have been predicted by thermal-structural analysis to assess the risk of through cracking in the hardening phase. The numerical simulation provides reliable insight into the temperature and stress evolution in massive concrete from the casting to 28 days when the properties of concrete are stabilized, and it is essential for the environmental and cost friendly design of the submerged concrete tunnel.

5.1. Numerical Method. The detailed numerical method is described in [28]. In the FE analyses, the thermal-structural problem is decoupled and solved in sequence by the finite element program DIANA. The temperature distribution over time is solved first, and these results are used as input for the subsequent stress calculation. The temperature gradient mainly depends on the total quantity of hydration heat, boundary conditions, thermal properties, and discontinuity in geometry and material properties. The stress gradient depends on temperature distribution, mechanical properties, restraint conditions, discontinuity in geometry and material properties, etc. It is more convenient to simulate the mass structure without reinforcement, and the results are conservative. In the current study, the steel reinforcement (bars, etc.) is not included in the numerical model.

Stress calculations need finer mesh than temperature calculations, the element in stress analysis has to be of higher order than the element in temperature analysis, and the requirements of stress analysis are usually decisive for element selection. The compatibility of the element type used in temperature and stress analysis is automatically handled by DIANA.

5.2. Finite Element Modelling. The tunnel consists of 50 sections, and the length of each section is 22 m. The cross section of the tunnel is not exactly symmetric, and the width between left side and middle wall is slightly different from the width between right side and middle wall. In the current study, the cross section is treated as symmetric, only half of the section is used in numerical analysis, it is considered that the simplification reduces the elements used in the finite element analysis (FEA) by 50%, and analysis results are still accurate enough for the design purpose. The boundary condition at the symmetry plane is fixed in the horizontal direction and has no heat transformation. The main dimensions of the tunnel structure are shown in Figure 4. The element mesh of the 3D model used in the analyses is shown in Figure 5. Due to symmetry conditions, only one-fourth of the structure between the dilation joints is modelled. The bottom slab is modelled as hardened concrete, while it is assumed that the walls and top slab are cast in one operation.

The boundary conditions used in analysis are the following:

(i) Fresh concrete temperature: 20°C

(ii) Ambient air temperature: 20°C

(iii) Wind velocity: 1 m/s

(iv) Vertical walls (21 mm plywood formwork; convectivity: 0.0033 kJ/m^{2}s°C)

(v) Top slab (plastic foil; convectivity: 0.0076 kJ/m^{2}s°C)

(vi) Time for formwork and plastic foil removal: 7 days (convectivity: 0.0133 kJ/m^{2}s°C)

The 20-node solid element CHX60 is used to model the concrete, and the element is automatically converted to 8-node HX8HT in the heat analysis. The 4-node boundary element BQ4HT is used to model the boundary conditions in the heat analysis.

6. Analysis Results and Discussion

The typical temperature and stress contour distribution in the middle section of the tunnel is shown in Figures 6 and 7 for SV concrete, and all the other four concrete types have

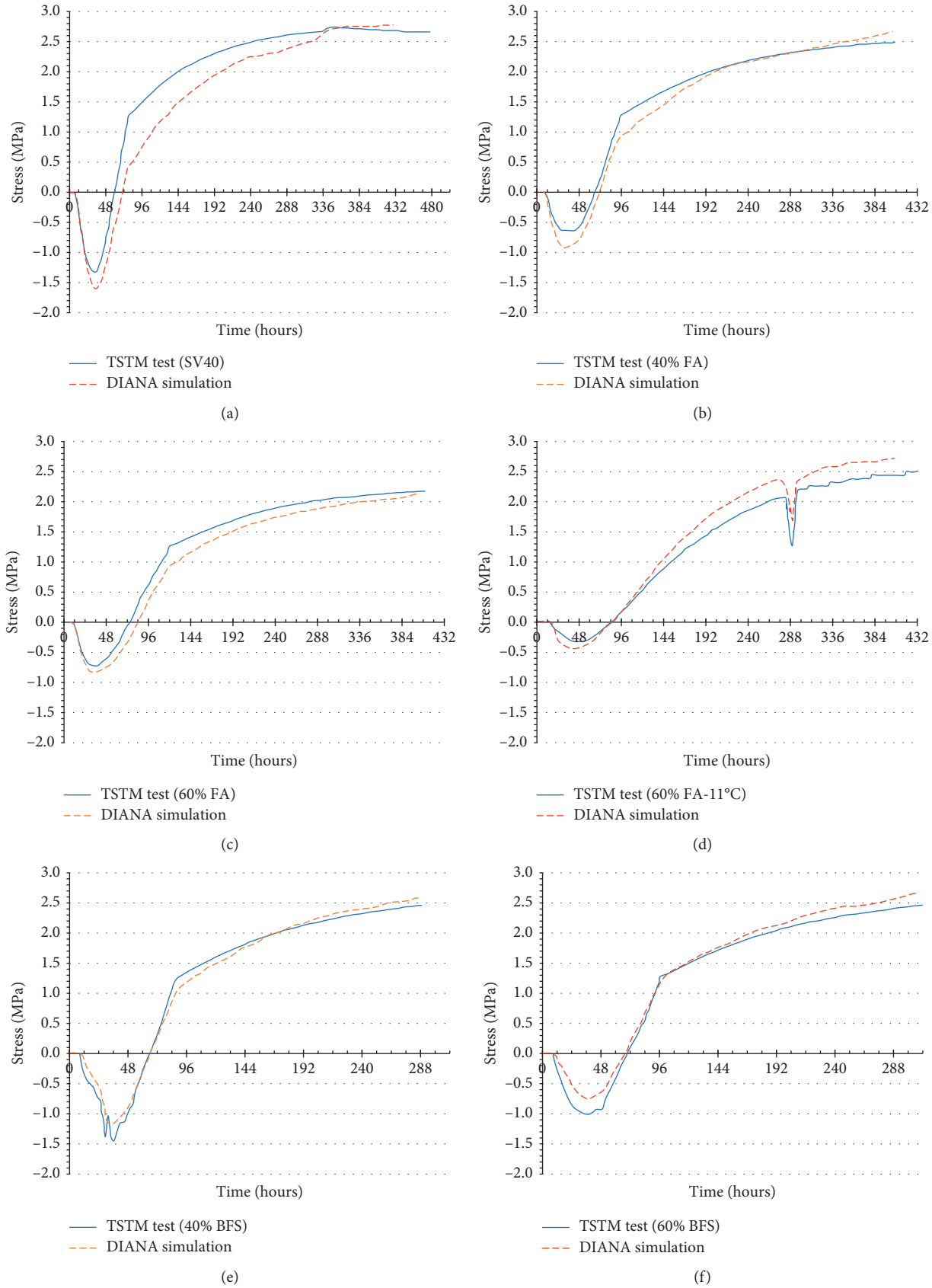

Figure 3: Calculated and measured stress development for the TSTM tests: (a) SV40; (b) 40% FA; (c) 60% FA; (d) 60% FA (11°C); (e) 40% BFS; (f) 60% BFS.

Table 6: Calculated and measured stresses in the TSTM tests.

Concrete type	Maximum compressive stress (MPa)				Maximum tensile stress (MPa)			
	Time (days)	TSTM	DIANA	Ratio	Time (days)	TSTM	DIANA	Ratio
SV40	1.5	1.27	1.59	0.79	15	2.75	2.72	0.99
40% FA	1.5	0.62	0.92	0.67	17	2.50	2.67	1.07
60% FA	1.6	0.70	0.82	0.85	17	2.17	2.16	1.00
60% FA-11°C	2	0.30	0.45	0.67	17	2.44	2.73	1.12
40% BFS	1.5	1.50	1.25	1.20	12	2.46	2.57	1.04
60% BFS	1.7	1.0	0.80	1.25	13	2.47	2.67	1.08

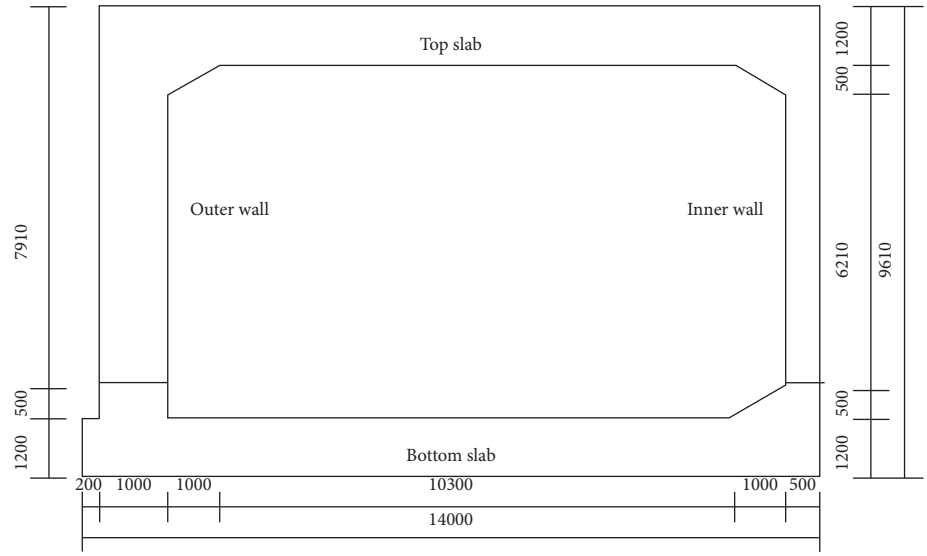

Figure 4: Geometry of the submerged tunnel (half of the cross section treated as symmetric).

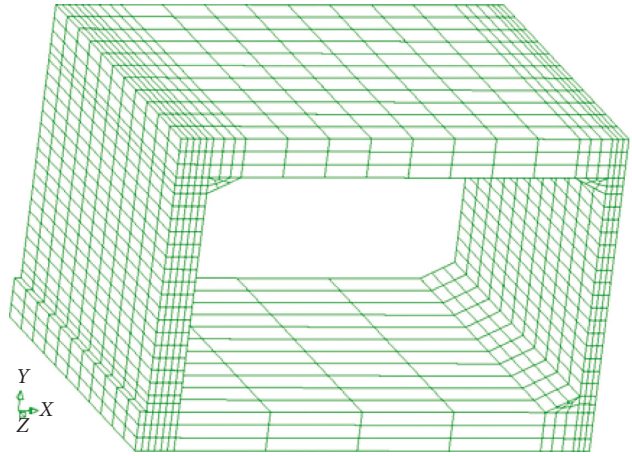

Figure 5: 3D finite element model of ¼ tunnel structure.

similar temperature and stress contour distribution. The maximum temperature appears at the corner between the inner wall and the top slab, while the critical locations, regarding the risk of through cracking determined as the ratio between maximum tensile stress and tensile strength, are in the center of the inner wall and approximately 0.6–1.2 m above the foundation slab. For the design of the submerged tunnel, the cracking in the outer wall is most critical to structure integrity and functionality, and the discussion of cracking risk will focus on the outer wall. In general, risk needs to take into account the hazard, exposure, and vulnerability over the time period. In the current study, the cracking risk is evaluated quantitatively, and the cracking index is defined as the ratio between stress

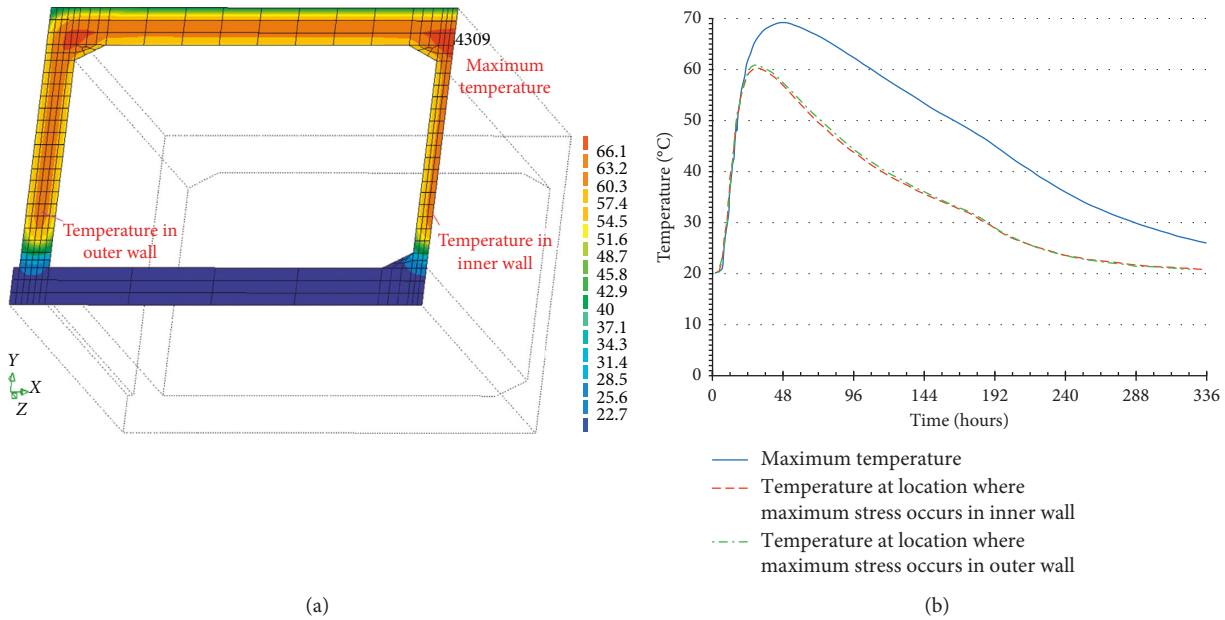

Figure 6: Calculated temperature developments of SV40 concrete: (a) temperature contour (48 h after casting); (b) maximum temperature in the structure and temperature developments in the inner and outer walls.

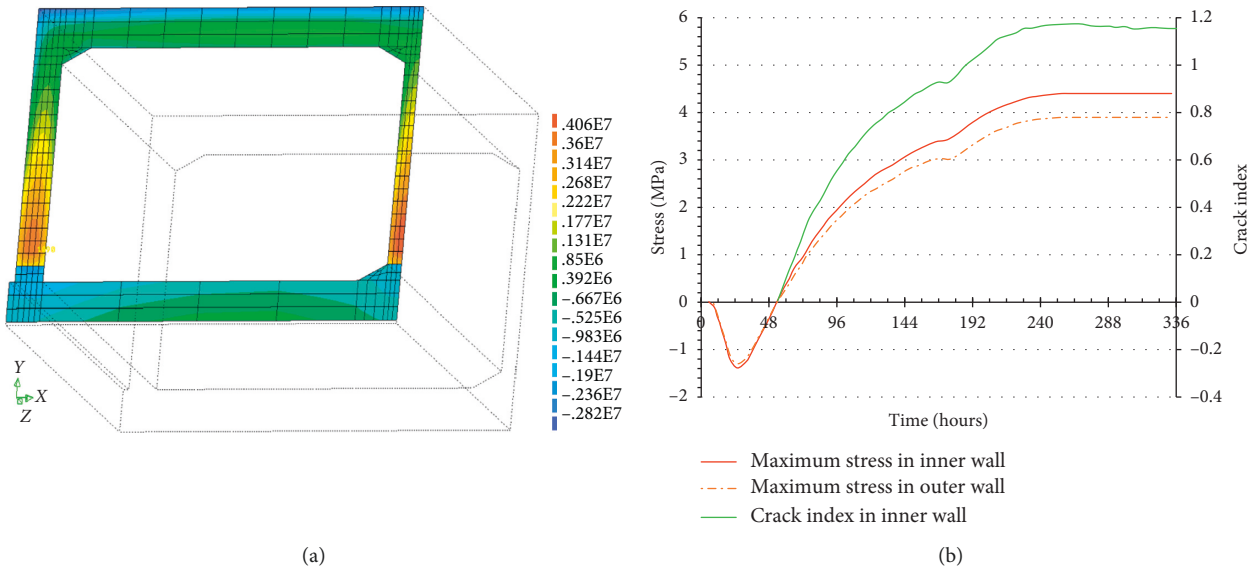

Figure 7: Calculated stress developments of SV40 concrete: (a) stress contour (336 h after casting); (b) stress developments in the inner and outer walls.

and tensile strength of concrete. The maximum temperatures in outer and middle walls, in addition to the maximum temperatures in the whole structure, are presented in Table 7.

The temperature and stress developments for 40% and 60% FA and 40% and 60% BFS concrete are shown in Figures 8–12. The calculated tensile strength after 2 weeks is presented in Table 8, and the corresponding stress/strength ratios at 14 days are summarized in Table 9 for the five types of concrete.

The results show that the risk of cracking is about 6–14% higher in the inner wall compared to the outer wall due to the higher degree of restraint in the inner wall, but the consequences of through cracking are most serious in the outer wall which therefore should have to meet the design crack criterion. It is seen that, for the initial temperature of 20°C, concrete with 60% FA achieves both the lowest maximum temperature (42.2°C/temperature rise 22.2°C) and the lowest risk of cracking (0.74) in the outer wall. The replacement of cement with FA or BFS reduces the maximum temperature and temperature rise significantly. The temperature rise at the critical location of the outer wall during hardening is 40.7°C for SV40 concrete, 26.5°C for 40% FA concrete, 25.6°C for 40% BFS concrete, and 24.9°C

Table 7: Calculated temperatures and the increase of temperature.

Concrete	Temperature (°C)					
	Outer wall		Inner wall		Whole structure	
	T_{max_out}	ΔT_{max_out}	T_{max_middle}	ΔT_{max_middle}	T_{max_whole}	ΔT_{max_whole}
SV40	60.7	40.7	60.3	40.3	69.0	49.0
40% FA	46.5	26.5	46.2	26.2	53.1	33.1
60% FA	42.2	22.2	41.9	21.9	48.4	28.4
60% FA-11°C	36.5	25.5	36.4	25.4	41.3	30.3
40% BFS	45.6	25.6	45.2	25.2	53.8	33.8
60% BFS	44.9	24.9	44.7	24.7	50.6	30.6

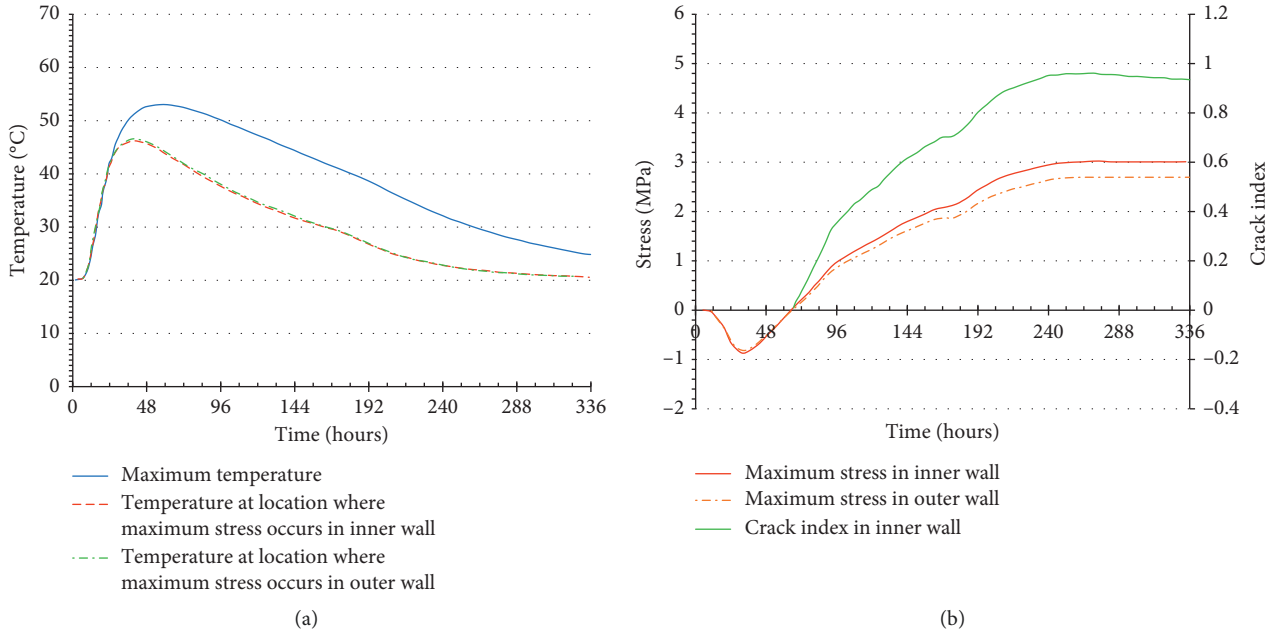

Figure 8: Calculated temperature (a) and stress (b) developments of 40% FA concrete.

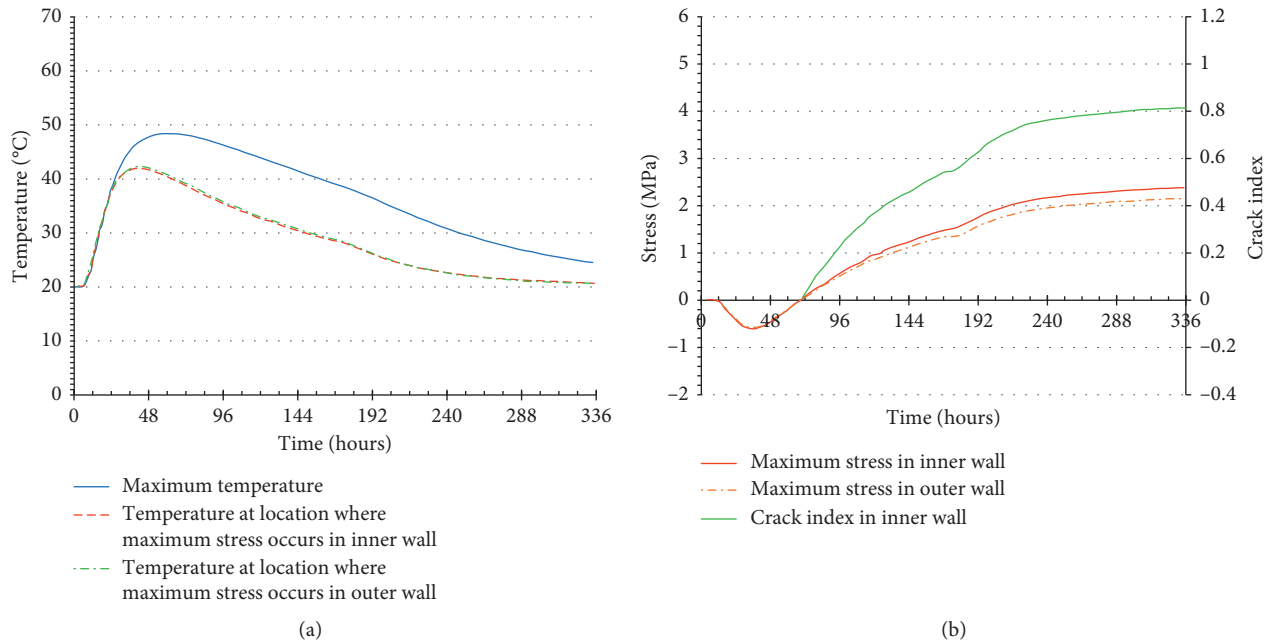

Figure 9: Calculated temperature (a) and stress (b) developments of 60% FA concrete.

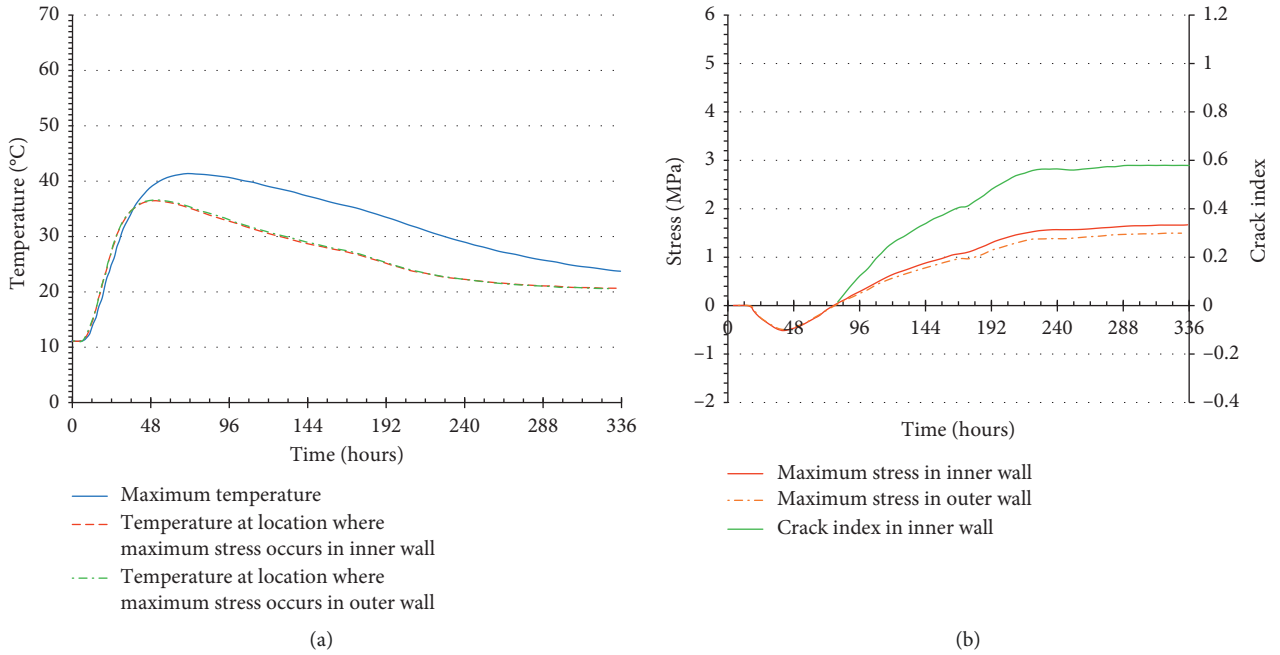

Figure 10: Calculated temperature (a) and stress (b) developments of 60% FA concrete with initial temperature 11°C.

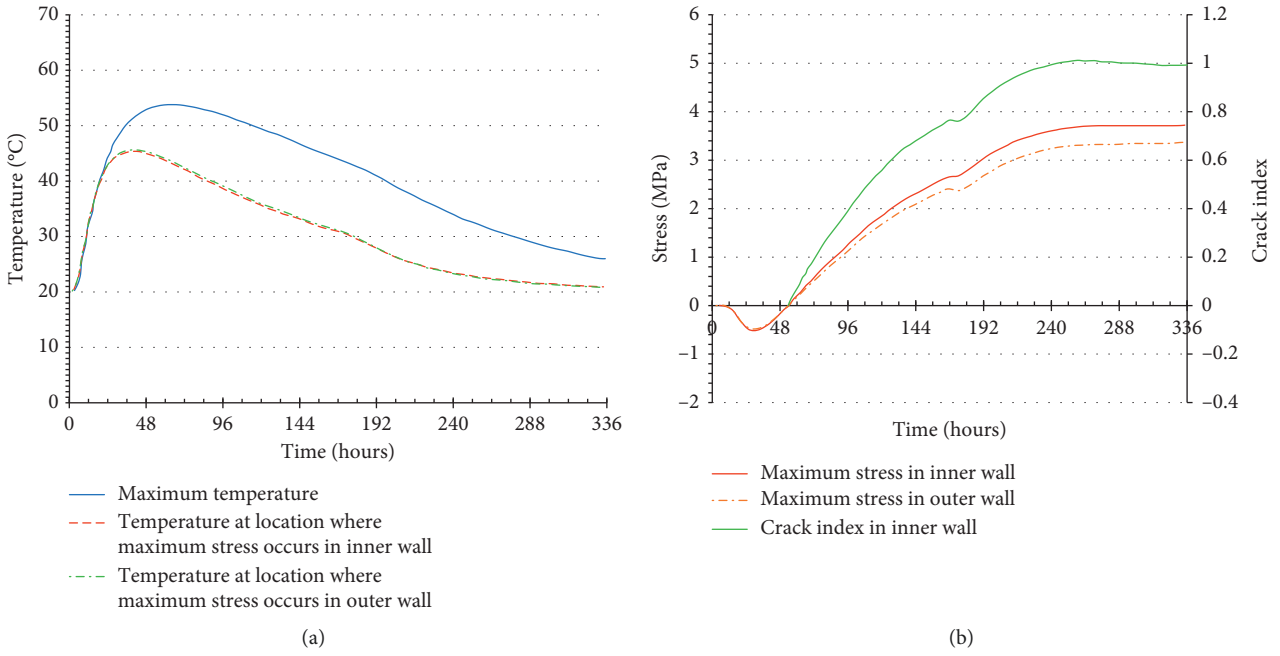

Figure 11: Calculated temperature (a) and stress (b) developments of 40% BFS concrete.

for 60% BFS concrete. The comparison of the crack index at the outer wall for different concrete is shown in Figure 13 and Table 9. Controlling of the initial temperature is the effective method to reduce the cracking risk for the massive concrete structure. The reduction of the fresh concrete temperature from 20 to 11°C results in a reduction of maximum temperature of 5.7°C, while the stress/strength ratio is reduced from 0.74 to 0.52 in the outer wall.

7. Conclusion

In the design of the massive concrete structure, the cracking risk in the hardening phase is the most critical for the integrity and durability of the structure. The proposed design methodology ensures that the appropriate composition of concrete is selected for the construction of the concrete submerged tunnel. The numerical method proposed here is

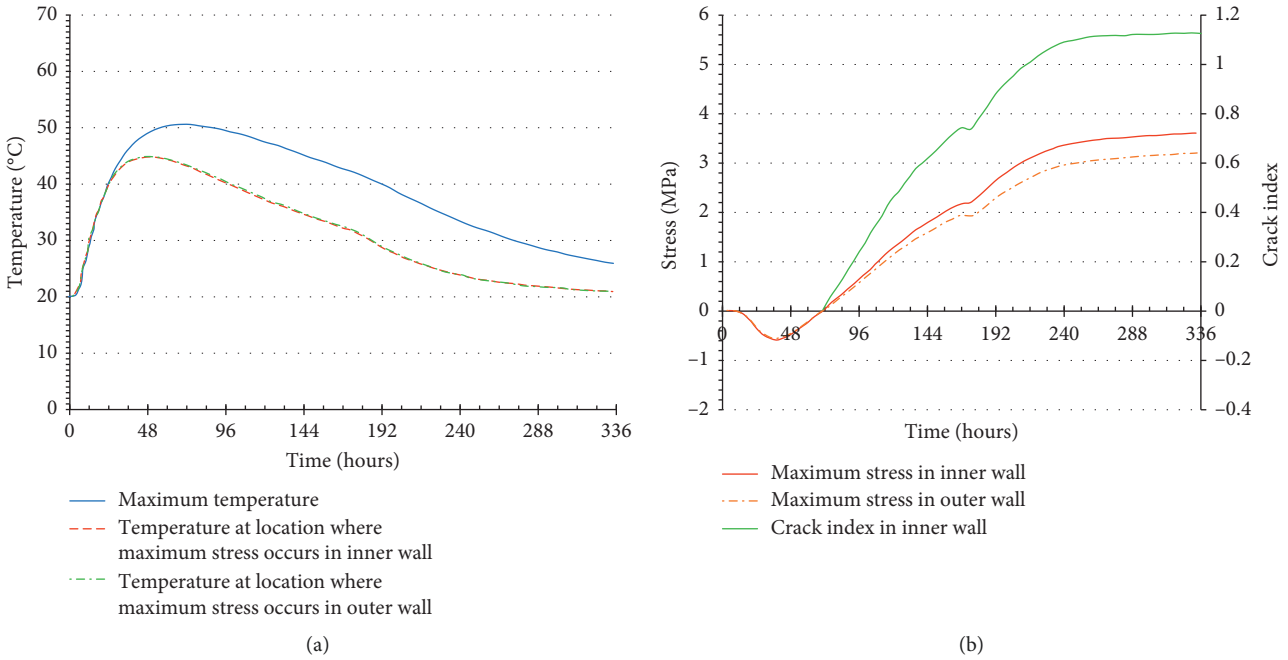

Figure 12: Calculated temperature (a) and stress (b) developments of 60% BFS concrete.

Table 8: Tensile strength at 14 days after casting.

Concrete	f_{t28} (N/mm^2)	Maturity time at 14 days after casting (days)	Tensile strength at critical time (N/mm^2)
SV40	3.86	22.2	3.79
40% FA	3.32	20.7	3.19
60% FA	3.00	22.5	2.91
60% FA-11°C	3.00	19.7	2.86
40% BFS	3.89	20.7	3.74
60% BFS	3.34	21.0	3.20

Table 9: Calculated stress/strength ratios at inner and outer walls at 14 days.

Concrete	Outer wall $\sigma_{tensile,\ max}$	Middle wall $\sigma_{tensile,\ max}$	Tensile strength	σ_t/f_t outer wall	σ_t/f_t inner wall
SV 40	3.91	4.40	3.79	1.04	1.18
40% FA	2.69	2.99	3.19	0.86	0.96
60% FA	2.14	2.38	2.91	0.74	0.82
60% FA-11°C	1.49	1.66	2.86	0.52	0.58
40% BFS	3.35	3.71	3.74	0.90	1.01
60% BFS	3.19	3.60	3.20	1.00	1.13

based on the finite element method, and it has the potential to be used as a design tool in the important submerged concrete tunnel project.

The risk of through cracking for the concrete submerged tunnel is determined for five types of concrete mixes denoted as SV40, 40% FA, 60% FA, 40% BFS, and 60% BFS concrete. The maximum temperature appears at the corner between the inner wall and the top slab, while the critical locations, regarding the risk of through cracking determined as the

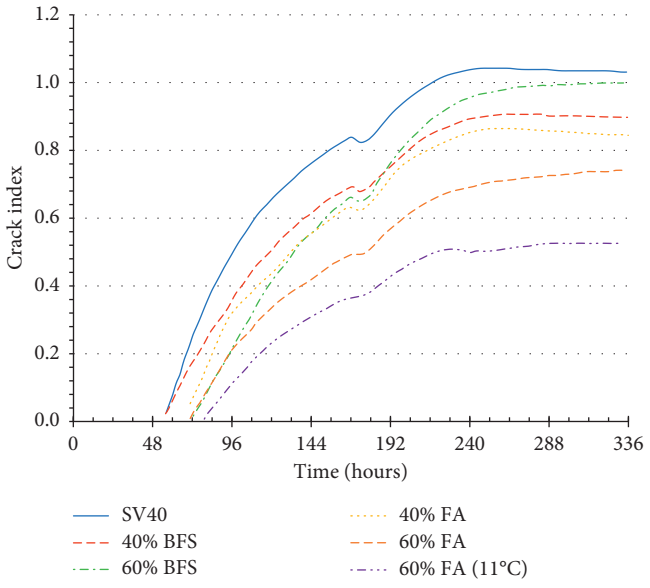

Figure 13: Crack index at the outer wall for different concrete.

ratio between maximum tensile stress and tensile strength, are at the center of the inner wall and approximately 0.6–1.2 m above the foundation slab. The temperature development is similar in the critical locations of the inner and outer walls, but the stresses and the risk of cracking are 12% higher in the inner walls due to a larger degree of restraint. However, only the outer wall will experience water pressure, and therefore, the results of the outer wall are given most attention. It is seen that concrete with 60% FA has both the lowest maximum temperature (42.2°C/temperature rise 22.2°C) and the lowest risk of cracking (0.74) in the outer wall. The temperature rise during hardening is 30.7°C

for SV40 concrete, 26.5°C for 40% FA concrete, 25.6°C for 40% BFS concrete, and 24.9°C for 60% BFS concrete. Furthermore, it is seen that the reduction in fresh concrete temperature from 20°C to 11°C results in a reduction of maximum temperature of 5.7°C, while the stress/strength ratio is reduced from 0.74 to 0.52.

Data Availability

The data used in the paper are accessible through the website https://brage.bibsys.no/xmlui/handle/11250/236401.

Conflicts of Interest

The authors declare that there are no conflicts of interest regarding the publication of this paper.

Acknowledgments

The financial contribution of the Norwegian Research Council is gratefully acknowledged. The NOR-CRACK partners were the Norwegian University of Science and Technology (project leader), Skanska Norge ASA, Elkem ASA Materials, Norcem AS, Fesil ASA, and the Norwegian Public Roads Administration. The paper is mainly based on the PhD project performed by Guomin Ji [19].

References

[1] S. Bernander and M. Emborg, "Risk of Cracking in Massiv Concrete Structures-New Development and Experiences," in *Proceedings of the RILEM International Symposium on Thermal Cracking in Concrete at Early Ages*, R. Springenschmid, Ed., pp. 385–392, E & FN Spon, London, UK, 1994.

[2] M. Emborg, "Thermal stresses in concrete structures at early ages," Doctoral thesis, Luleå University of Technology, Luleå, Sweden, 1989.

[3] J. R. Wright, F. Rajabipour, J. A. Laman, and A. Radlińska, "Causes of early age cracking on concrete bridge deck expansion joint repair sections," *Advances in Civil Engineering*, vol. 2014, Article ID 103421, 10 pages, 2014.

[4] P. Havlásek, V. Šmilauer, K. Hájková, and L. Baquerizo, "Thermo-mechanical simulations of early-age concrete cracking with durability predictions," *IOP Conference Series: Materials Science and Engineering*, vol. 236, 2017.

[5] A. B. E. Klausen, *Early age crack assessment of concrete structures: experimental determination of decisive parameters*, Ph.D. thesis, NTNU, Trondheim, Norway, 2016, ISBN 978-82-326-1850-7.

[6] IPACS, "Brite-Euram project BRPR-CT97-0437," Improved Production of Advanced Concrete Structures, 1997-2001.

[7] J. Olofsson and M. Uhlán, *Round Ronbin Simulation–Ground Slab Examples*, ISBN 91-89580-54-0, Skanska Teknik AB, Stockholm, Sweden, ISBN 91-89580-54-0, 2000.

[8] R. Springenschmidt, *Thermal Cracking in Concrete at Early Ages, Proceedings of the International RILEM Symposium*, E&FN Spon, London, UK, 1995.

[9] R. Springenschmidt, R. Breitenbucher, and M. Mangold, *Development of the Cracking Frame and Temperature Stress Testing Machine, Thermal Cracking in Concrete at Early-Age*, EF Spon, London, UK, 1994.

[10] A. B. E. Klausen, T. Kanstad, Ø. Bjøntegaard, and E. Sellevold, "Comparison of tensile and compressive creep of fly ash concretes in the hardening phase," *Cement and Concrete Research*, vol. 95, pp. 188–194, 2017.

[11] A. B. E. Klausen, T. Kanstad, and Ø. Bjøntegaard, "Updated Temperature-Stress Testing Machine (TSTM): introductory tests, calculations, verification and investigation of variable fly ash content," in *Proceedings of International Conference: Concreep-10 Mechanisms and Physics of Creep, Shrinkage, and Durability of Concrete and Concrete Structures*, p. 9, Vienna, Austria, September 2015.

[12] C. K. Rankoth, A. Hosoda, and K. Iwama, "Modeling and verification of early age thermal stress in second lining concrete of NATM tunnels," *Journal of Advance Concrete Technology*, vol. 15, no. 6, pp. 213–226, 2017.

[13] M. S. Sule and K. van Breugel, "Effect of reinforcement on early-age cracking in high strength concrete," *HERON*, vol. 49, no. 3, 2004.

[14] E. Strieder, R. Hilber, E. Stierschneider, and K. Bergmeister, "FE-study on the effect of gradient concrete on early constraint and crack risk," *Applied Sciences*, vol. 8, no. 2, p. 246, 2018.

[15] B. Klemczaka, M. Batogb, M. Pilcha, and A. Zmij, "Analysis of cracking risk in early age mass concrete with different aggregate types," in *Proceedings of International Conference on Analytical Models and New Concepts in Concrete and Masonry Structures AMCM'2017*, 2017.

[16] J. Fu, Y. Wu, and Y.-b. Yang, "Effect of reinforcement strength on seismic behavior of concrete moment frames," *Earthquake and Structures*, vol. 9, no. 4, pp. 699–718, 2015.

[17] B. Hu, J. Wang, and G. Li, "Numerical simulation and strength models of FRP-wrapped reinforced concrete columns under eccentric loading," *Construction and Building Materials*, vol. 25, no. 5, pp. 2751–2763, 2011.

[18] A. I. Karabinis, T. C. Rousakis, and G. E. Manolitsi, "3D finite-element analysis of substandard RC columns strengthened by fibre reinforced polymer sheets," *Journal of Composites for Construction*, vol. 12, no. 5, pp. 531–540, 2008.

[19] G. M. Ji, "Cracking risk of concrete structures in the hardening phase: experiments, material modelling and finite element analysis," Doctoral thesis, NTNU, Dept. of Structural Eng., Norway, 2008.

[20] P. F. Hansen and E. J. Pedersen, "Maturity computer for controlled curing and hardening of concrete," *Nordisk Betong*, vol. 1, no. 19, pp. 21–25, 1977.

[21] T. Kanstad, T. A. Hammer, Ø. Bjøntegård, and E. J. Sellevold, "Mechanical properties of young concrete: Evaluation of test methods for tensile strength and modulus of elasticity," Determination of model parameters, SINTEF-report no. STF22 A99762, Trondheim, 1999.

[22] Z. P. Bažant and L. Panula, *Simplified Prediction of Concrete Creep and Shrinkage From Strength and Mix, Structural Engineering Report, No. 78-10/6403*, Department of Civil Engineering, Technological Institute, Northwestern University, Evanston, IL, USA, 1978.

[23] Z. P. Bažant and L. Panula, "Practical prediction of time dependent deformations of concrete," *Materials and Structures, Part I and II*, vol. 11, no. 5, pp. 307–328, 1978.

[24] T. Kanstad, T. A. Hammer, Ø. Bjøntegaard, and E. J. Sellevold, "Mechanical properties of young concrete: Part 1:Experimental results related to test method and temperature effects," *Materials and Structures*, vol. 36, no. 258, pp. 218–225, 2003.

[25] T. Kanstad, T. A. Hammer, Ø. Bjøntegaard, and E. J. Sellevold, "Mechanical properties of young concrete: Part 2: Determination of model parameters and test program proposals," *Materials and Structures*, vol. 36, no. 4, pp. 226–230, 2003.

[26] Ø. Bjøntegaard, T. A. Hammer, and E. J. Sellevold, "On the measurement of free deformation of early age cement paste and concrete," *Cement and Concrete Compositions*, vol. 26, no. 5, pp. 427–435, 2004.

[27] *DIANA FEA User's manual*, DIANA FEA BV, 2017.

[28] G. M. Ji, T. Kanstad, and Ø. Bjøntegaard, "Numerical modelling of field test for crack risk assessment of early age concrete containing fly ash," *Advances in Materials Science and Engineering*, vol. 2018, Article ID 1058170, 16 pages, 2018.